ELSEVIER

Journal of Power Sources 63 (1996) 235–246

JOURNAL OF POWER SOURCES

Hydrogen and oxygen evolution in sealed lead/acid 2 V cells. In situ gas measurement by Raman spectroscopy

F.E. Henn [a,*], C. Rouvet [b], A. de Guibert [b], Ph. Marteau [c]

[a] *Laboratoire de Physico-Chimie de la Matière Condensée, UMR C 5617, Université de Montpellier II, place Eugène Bataillon, 34095 Montpellier Cedex 05, France*

[b] *Compagnie Européenne d'Accumulateur (CEAC), 5–7 allée des Pierres Mayettes, 92636 Gennevilliers Cedex, France*

[c] *Laboratoire d'Ingeniérie des Matériaux et Hautes Pressions, Institut Galilée, avenue J.B. Clement, 93430 Villetaneuse, France*

Received 25 September 1996; accepted 30 September 1996

Abstract

Hydrogen, oxygen, nitrogen pressures inside five sealed lead/acid 2 V cells of 10 Ah are measured by Raman spectroscopy. Gas evolution is determined during short-term overcharge and rest periods. During the rest period, the oxygen reduction rate is in agreement with recently published data. Using qualitative data, it seemed that during overcharge, the oxygen reduction does not totally hinder the hydrogen evolution which is consequently much higher than expected. However, we observed that in our case hydrogen evolution is not correlated with the oxygen reduction rate assuming that the oxygen cycle is not fully accomplished, though oxygen reduction takes place. As a consequence and for evident balance of current, hydrogen evolution increased. Possible explanations are: mixed potential at the negative electrodes; grid corrosion, or oxidation of organic impurities at the positive electrodes.

Keywords: Lead/acid batteries; Hydrogen evolution; Oxygen revolution

1. Introduction

In order to prevent emission of gas and therefore be able to construct sealed or valve-regulated lead/acid (VRLA) batteries that would be ideally maintenance-free or 'zero-gas emission', many investigations are undertaken on the evolution of hydrogen and oxygen and on recombination reactions. Reviews of early investigations are published by Bose and Hampson [1], Mrha et al. [2], Nelson [3] and more recently by Bernt [4].

Because of the limited understanding of gas-evolution mechanisms and the resulting uncontrolled life expectancy of VRLA batteries [5] further studies are needed.

Bodoardo et al. [6] provided a new insight into the subject and underlined some of the most important reactions featuring oxygen and hydrogen cycles in gas-recombinant lead/acid systems.

In the following, we will refer to 'oxygen recombination' when the oxygen cycle is totally achieved, e.g. no water loss — whatever the mechanism considered — and to 'oxygen reduction' when only the reduction of oxygen at the negative plate is taken into account. Oxygen reduction does not mean that the oxygen cycle is completely achieved.

In order to study these mechanisms, the authors should analyse current, voltage, pressure and gas composition measurements. Although the three first parameters are easily monitored without modifying the system studied, gas composition measurement appears to be a more difficult task. When gas chromatography is used [6–9], it is necessary to sample a volume of gas and to wait several minutes before re-sampling. This procedure has several disadvantages:

1. Gas sampling is not easy to perform under very low (few kPa) or very high pressures, air contamination or gas loss being possible.
2. Gas released into the upper part of the battery may not have the exact composition of gas contained in the whole free volume, including gas trapped in plates and separator voids.
3. In the course of gas sampling, it is possible to affect the internal pressures and therefore to change the kinetics of multiple reactions. This problem can be avoided when the free volume of the battery is large compared with the volume of gas needed for analysis. This requirement is difficult to satisfy with small capacity batteries or single plate studies, when we do not want to change drastically

* Corresponding author.

PII S0378-7753(96)02480-9

the factor-of-merit [6] between the plate surface and the free volume of the studied cell available to gases compared with a standard accumulator.

4. For the above reasons, frequent sampling cannot be achieved and accurate kinetics cannot be assessed.

In this paper, a new experimental approach is proposed, based on Raman spectroscopy, in order to measure in situ hydrogen and oxygen pressures. Using a suitable experimental setup and calibration, we were able to monitor the gas composition every minute. More than 600 spectra were recorded for the determination of the evolution of gas.

We modified the container of standard 2 V VRLA/absorptive glass mat (AGM) cells, making them airtight up to 0.5 MPa, thus allowing in situ measurement to be made. Only a minor discrepancy is obtained between pressures measured via a pressure sensor and those measured via Raman spectroscopy.

In addition to the experimental description, we propose a qualitative interpretation of the results. Although some of the interpretations may be questionable, especially due to the second disadvantage listed above, we think that this first experimental approach can be greatly improved and could give some new qualitative and quantitative information.

2. Experimental

2.1. Optical setup

A schematic diagram of the optical system is shown in Fig. 1. The gas mixture is illuminated by the green light (514.53 nm) of an argon laser. The Raman scattered signal is collected at the entrance of a Dilor spectrometer. The spectra delivered to the computer are then analysed through a purpose-designed program to give the relative gas concentrations. The Raman signals from gases at low pressures are so weak that an excitation power as high as 600 mW is required together with an acquisition time as long as 120 s. Consequently, a flat background is more easily obtained with a right angle scattering configuration rather than with the back-scattered configuration commonly used on most spectrometers. A typical example of the Raman spectra obtained is given in Fig. 2. In order to capture the whole spectrum at once, i.e. without rotation of the grating, a second Dilor monochromator has been used. The latter, equipped with a 600 g/mm grating, has a focal length of 250 mm. As a consequence of the rather low dispersion of the spectrum on the charge coupled device detector, the vibrational lines extend over approximately 10 pixels only. However, the partial pressures deduced from their measured integrated intensities are still accurate enough when the calibration has been carried out under the same conditions.

2.2. Quantification

The determination of partial pressures is based upon the linear relationship that exists between the Raman intensity and the concentration of molecules, i.e. the partial pressure, as long as the latter is low enough. This relationship can be expressed as

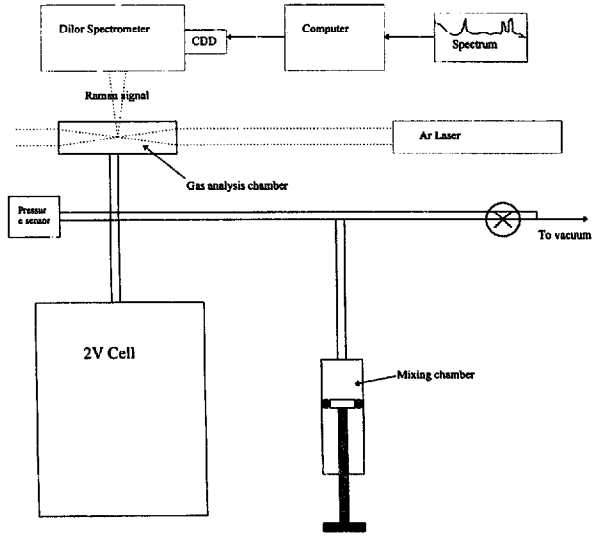

Fig. 1. Schematic representation of the experimental setup.

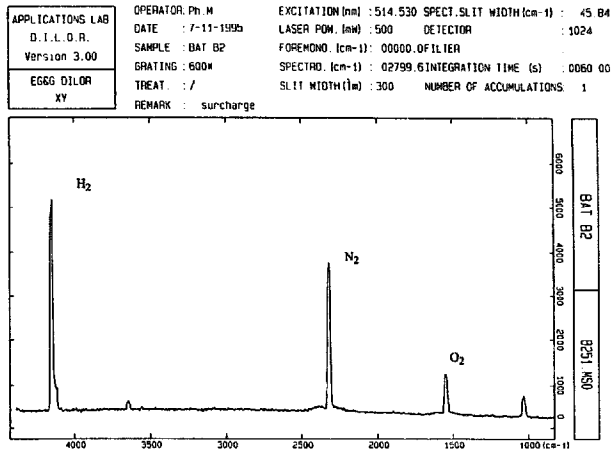

Fig. 2. Typical Raman spectrum obtained on the cell B with $P_{O_2} = 28.5$ kPa, $P_{H_2} = 60.5$ kPa, and $P_{N_2} = 100$ kPa.

$$A_X = C_X P_X \quad (1)$$

where A_X is the Raman integrated intensity, P_X the partial pressure and C_X the coefficient of proportionality. Because these coefficients depend on many factors, such as the excitation power, the optical geometry at the entrance of the spectrometer, etc., their absolute values cannot easily be determined. For that reason, all measurements were referred to that of nitrogen, whose partial pressure was constant and equal to the atmospheric pressure. Then, the partial pressures of hydrogen and oxygen were calculated by applying the following relations:

$$P_{H_2}/P_{N_2} = C_{H_2/N_2} \times A_{H_2}/A_{N_2}$$
$$P_{O_2}/P_{N_2} = C_{O_2/N_2} \times A_{O_2}/A_{N_2} \quad (2)$$

where the coefficients C_{H_2/N_2} and C_{O_2/N_2} have been previously determined from the calibration spectra of mixtures of these gases with known concentrations.

2.3. Calibration

Three sets of six mixtures, leading to 18 different mixtures, were prepared in the following way: the evacuated optical cell was first partially filled with hydrogen at pressures of 2, 4 and 6 psi, respectively (1 psi = 6.8918 kPa). In each case the cell was then filled up to 100 kPa with atmospheric air. Then, the total pressure was reduced to 93.1, 82.7, 68.9, 41.3 and 27.6 kPa by pumping in stages. For each of these 18 mixtures the integrated intensities of the Raman lines were measured. From an examination of these values we can conclude that the relative pressures can be determined with an uncertainty of approximately 3 or 4%.

3. Cell design

Investigations were carried out on 2 V cells using the VRLA/AGM technology. The cells were filled with five different electrolyte compositions, see Table 1. These compositions are not much different from each other since we wanted to be close to usual industrial conditions.

The cells were assembled with 7 negative and 6 positive plates separated by a standard absorptive microfibre glass mat. In order to limit the dispersion of data, plate weights, thickness and dimensions of the plates were checked carefully. The plates were selected among a large set of plates provided by one of the CEAC plants and manufactured from the same lot of unformed active mass. The negative and positive tribasic sulfate-based active masses had standard chemical and physical characteristics. The electrolyte was a solution of sulfuric acid, water and sodium sulate (8 g/l) in water. Under standard conditions, the mean C_{20} capacity was about 10 Ah, see Table 2.

Forafac 1033 D which is a 30% aqueous solution of polyfluorosulfonic acid surfactant provided by Atochem is known

Table 1
Characteristics of cells regarding the electrolyte

Type	Volume of electrolyte (cm^3)	Electrolyte specific gravity (g/cm^3 at 20 °C)	Additives in the electrolyte
A	97	1.30	
B	97	1.30	1 g/l of Forafac 1033D
C	97	1.33	
D	97	1.27	
E	99	1.30	

Table 2
Discharge and recharge parameters for each cell measured prior to gas evolution experiments

Cell	C_{20} (Ah)	% recharge coefficient	End of charge current (mA)
A	11.6	105	6
B	11.1	107	7
C	12.9	106	8
D	10.4	107	7
E	12.1	105	4

to reduce gas emission [10,11]. Gas-emission inhibitors have been the subject of recent publications and could be one way to reduce the amount of gas evolved [12,13]. As oversoaking can strongly hinder oxygen recombination [2,14], it is therefore very important to compare 2 V cells soaked with exactly the same volume of electrolyte.

The influence of the specific gravity (sp. gr.) of the acid on the gas evolution has to be verified. As far as we know, oxygen diffusion at the active mass/electrolyte/gas interface is the rate-determining step for oxygen recombination. It depends on the oxygen solubility in the electrolyte and it is well known that the higher is the sp. gr. of the acid the lower is the solubility and the oxygen recombination rate. Likewise, it must be kept in mind that the increase in sp. gr. of the acid enhances the sulfation rate (or self-discharge) of the active mass and, as a consequence, favours hydrogen and oxygen emission. Further, increasing the sp. gr. of the acid modifies the corrosion of the positive grid [15].

First, these cells were equipped with standard valves, which have an opening pressure of about 10 to 15 KPa above the atmospheric pressure and were submitted to a C_{20} discharge control test followed by a 24 h voltage-limited recharge at 2.5 A and 2.4 V. Results are given in Table 2.

Second, as expected, high sp. gr. and oversoaking improve capacity, whereas — because it hinders recombination — oversoaking decreases the end of charge current.

Then, sealing these cells, we replaced the standard valves by airtight (up to 1 MPa) valves as used in automobile tyre technology and covered the entire cell with a 1–2 cm thick layer of vinyl ester resin (Fig. 3).

The cells were able to sustain, at least, an internal gas pressure of 0.5 MPa without mechanical deformation. Several measurements showed that the gas leakage was less than 0.1 kPa/h, provided that the free volume is about 35 cm^3.

We attempted to measure the in situ gas composition. For that purpose, we placed two glass windows on the opposite sides of the cell, allowing the laser beam to cross the empty space above the plates. Unfortunately, due to acid mist and drops onto the glass windows, the emission signal was absorbed and the analysis of the gas was not possible. Therefore, we were forced to use another experimental setup, as described in Section 2, where gases were analysed in a chamber connected to the 2 V cell. Although, it does not correspond, strictly speaking to 'real' in situ conditions, it has

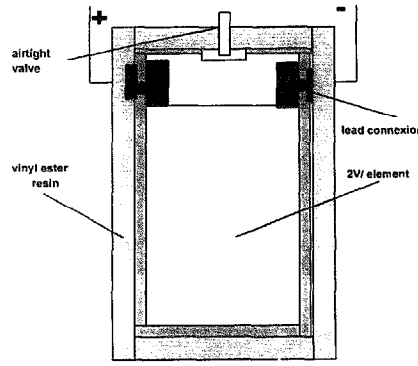

Fig. 3. Schematic representation of a sealed cell.

some advantages compared with the usual gas sampling method, i.e. gas chromatography.

When the first cell studied was charged, we observed a pressure increase (pressure sensor) that did not correspond with the evolution of the Raman spectra. Nitrogen pressure was increasing instead of the hydrogen and oxygen pressures. We, then, assume that gas diffusion towards the analysis chamber was not fast enough and that a significant heterogeneity in the gas composition was responsible for this observation. This means that in complex geometric systems, such as electrochemical cells or accumulators, gases released are unlikely to be easily mixed. We added a chamber to our setup where gases had to be homogenized. By a succession of compression/decompression cycles, part of the gas trapped in the porosity was likely to be released and mixed with the gases present in the upper part of the cell. This homogenization must not suggest that the gas evolution law can be disturbed by pressure changes, as elucidated in Section 1, see disadvantage 3. However, Fig. 4 shows that the pressure trends, measured both from the pressure sensor and Raman spectroscopy, are comparable, thus indicating that the mixing procedure allows a good homogeneity of gases.

4. Test procedure

Prior to measurement, each cell was overcharged for about 12 h at 2.4 V, connected to the experimental apparatus, emptied to less than 0.1 kPa and refilled with pure nitrogen up to 0.1 MPa.

Then the following steps were applied:

1. overcharge at constant current i for 1 h;
2. rest period for at least 2 h, and
3. emptying and refilling with pure nitrogen to 0.1 MPa

Three cycles were successively undertaken at $i = 0.2$, 0.4 and 0.6 A. In some cases, we had to stop the 0.6 A overcharge

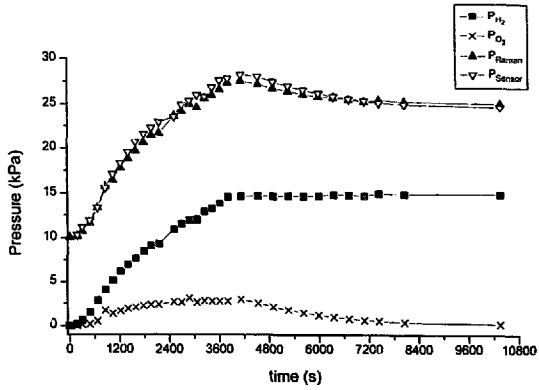

Fig. 4. Comparison between the total pressure measured via pressure sensor and the sum of hydrogen, oxygen and nitrogen pressure calculated via Raman signal. Cell C overcharge and rest period.

within 1 h when the internal pressure reached more than 0.4 MPa.

The goal of this procedure was to assess the oxygen–reduction rate during the rest period and the kinetics of hydrogen and oxygen evolution during the previous overcharge. Correlation between the gas evolutions are investigated and discussed in the next sections.

For such recombination mechanisms, steady state may be reached after more than 1 or 2 h [6], depending on many factors because gas transport through the separator and the plate porosity is governed by complex and slow processes. Likewise, oxygen reduction on negative plates may enhance any plate potential inhomogenities [16,17] which take time to reach a stationary state. Meanwhile, reaching a steady state, if possible, would require that gas loss due to leakages through the walls of the cell and the experimental setup be much less than the slowest gas evolution rates.

5. Theoretical concepts

5.1. Equations of gas evolution during the rest period

As a result of oxygen reduction on lead, the oxygen pressure decreases rapidly. Under open-circuit voltage (OCV), this reaction can be expressed as

$$Pb + \frac{1}{2}O_2 + H_2SO_4 = PbSO_4 + H_2O \quad (3)$$

obeying the general kinetic law

$$v_{O_2(red)} = \frac{dP_{O_2}}{dt} = -K_{O_2}(t)[P_{O_2}]^{n(t)} \quad (4)$$

If the reaction obeys a simple elementary mechanism, the oxygen reduction rate constant $K_{O_2}(t)$ and kinetic parameter $n(t)$ are time constants and n equals 1. In that case, K_{O_2} is the slope of the logarithm of the oxygen pressure $\log(P_{O_2})$ as function of time, t, according to

$$P_{O_2}(t) = P_{O_2}^{init}\exp(-K_{O_2}t) \quad (5)$$

where $P_{O_2}^{init}$ is the oxygen pressure at $t=0$. Bodoardo and al. [6] pointed out that Eq. (5) is followed as long as t does not exceed 1 or 2 h. Then, other effects, such as plate structure modification and the slow diffusion through the negative mass, slowly decrease the rate of the reaction (3).

In our case, hydrogen and oxygen evolution due to self-discharge of the positive and negative active mass are much slower than oxygen reduction and thus do not influence the measurement of the oxygen pressure decay. However, in experiments that last much longer (at least 24 h) and when most of the oxygen is reduced, gas emission due to self-discharge can be easily observed.

5.2. Equations of gas evolution during overcharge

Assuming the cell is fully charged, the constant current, i, equals:

(i) *at the positive electrodes*

$$i = i_{O_2(gas)} + i_{(misc)} \quad (6)$$

where $i_{O_2(gas)}$ is the current corresponding to the oxygen formed at the positive plate and $i_{(misc)}$ represents miscellaneous reactions such as grid corrosion, oxidation of organic species (plastic fibres, additives,···). For instance, carbon dioxide emission was commonly observed [7].

In a recombinant cell $i_{O_2(gas)}$ is usually split into

$$i_{O_2(gas)} = i_{O_2(rel)} + i_{O_2(red)} \quad (7)$$

where $i_{O_2(rel)}$ is related to the oxygen released into the empty space of the cell and measured via the Raman signal. $i_{O_2(red)}$

corresponds to the oxygen evolved at the positive electrode and reduced at the negative electrode. As already outlined, discrepancies may arise between $i_{O_2(rel)}$ and the oxygen pressure measured via Raman spectroscopy due to gases trapped in porosity; it is, however, very difficult to assess this possible difference accurately. In a first stage and according to our experimental setup and procedure, we assume that this difference is negligible.

In a good recombinant system and for overcharge currents that are lower than the limiting recombinant current [2,6] — usually comprised between 1 and 3 mA/cm² of negative plate — $i_{O_2(rel)} < i_{O_2(red)}$ and the oxygen pressure tends to low value. Otherwise, when the oxygen reduction rate constant K_{O_2} and the resulting $i_{O_2(red)}$ is small compared with the overcharge current, i, the oxygen pressure increases more rapidly.

(ii) *at the negative electrodes*

$$i = i_{H_2(gas)} + i_{O_2(rec)} \tag{8}$$

where $i_{H_2(gas)}$ is the current corresponding to the hydrogen evolution and $i_{O_2(rec)}$ corresponds to the oxygen recombined at the negative electrode.

For the following calculations and discussion, we assumed that hydrogen oxidation [6] was negligible and that $i_{H_2(gas)}$ was equal to $i_{H_2(rel)}$, the hydrogen released into the free volume of the cell. Likewise, in a first approximation, it is generally assumed that all the oxygen reduced is equivalent to the oxygen recombined and that $i_{O_2(rec)} = i_{O_2(red)}$. Therefore Eqs. (6)–(8) lead to

$$i_{H_2(rel)} = i_{O_2(rel)} + i_{(misc)}$$

or

$$\frac{i_{H_2(rel)}}{i_{O_2(rel)}} = 1 + \frac{i_{(misc)}}{i_{O_2(rel)}} \tag{9}$$

This relation is valid whatever $i_{O_2(rec)}$ and the overcharge current, i, and it reveals that the ratio $i_{H_2(rel)}/i_{O_2(rel)}$, hence the gas composition, strongly depends on the ratio $i_{(misc)}/i_{O_2(rel)}$ that increases when $i_{O_2(rel)}$ is low. However, it must be kept in mind that, according to our overcharge procedure, $i_{O_2(rel)}$ remains in all cases much higher than $i_{(misc)}$ which is often considered to be of the order of several μA.

5.3. Relations between gas evolution and current during charging

In adiabatic and isothermal conditions, the oxygen and hydrogen evolution $v_{O_2(rel)}$ and $v_{H_2(rel)}$ are simply related to the corresponding current

$$i_{O_2(rel)} = 4Av_{O_2(rel)} \quad \text{and} \quad i_{H_2(rel)} = 2Av_{H_2(rel)} \tag{10}$$

with $A = VF/RT$ and $F = 96\,500$C.

The determination of the free volume, V, is not accurate and can give important errors when we want to calculate oxygen or hydrogen currents from the experimental measurements of $v_{O_2(rel)}$ and $v_{H_2(rel)}$. We, then, prefer to deal with the ratio $i_{H_2(rel)}/i_{O_2(rel)}$ or $v_{H_2(rel)}/v_{O_2(rel)}$ which eliminates the factors influencing Eq. (10).

From Eqs. (9) and (10), we obtain

$$\frac{v_{H_2(rel)}}{v_{O_2(rel)}} \geq 2 \tag{11}$$

If all the relations were correct, we should observe that:

1. As often suggested, during overcharge, the higher is the oxygen reduction rate, the lower is $v_{O_2(rel)}$ and $v_{H_2(rel)}$, according to Eqs. (7) and (8).
2. Whatever the oxygen reduction rate, the ratio between hydrogen and oxygen evolution must be equal to or slightly higher than 2 (Eq. (11)).
3. However, the higher oxygen reduction rate and the lower the oxygen evolution, the higher are the effects of corrosion and others miscellaneous reactions on gas stochiometry, i.e. departure from the value of 2 (Eq. (11)) is higher.

6. Results and discussion

6.1. Determination of the reduction rate

In Fig. 5 typical P_{O_2} evolution after 1 h overcharge is given. In all cases the parameter n turns out to be close to 1 and according to Eq. (5). K_{O_2}, $P_{H_2}^{init}$, $P_{O_2}^{init}$ are reported in Table 3.

We attempt to find a correlation between the reduction rate constant and the initial oxygen and hydrogen pressures, the previous overcharge current, i, and the type of cell. Only K_{O_2} exhibits a good correlation with the initial oxygen pressure (Fig. 6). This correlation results from the first remark in Section 5.3, since the oxygen evolution during the previous overcharge depends on the oxygen reduction rate constant. In contrast, K_{O_2} seems not be well correlated with the initial hydrogen pressure (Table 3). Also, there is no obvious correlation between the overcharge current and K_{O_2}, indicating

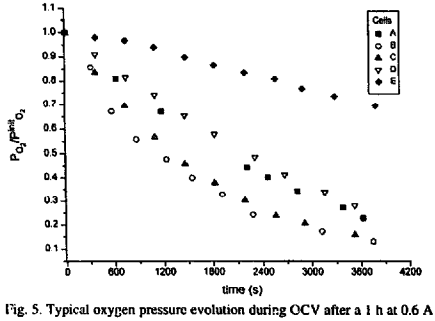

Fig. 5. Typical oxygen pressure evolution during OCV after a 1 h at 0.6 A overcharge. The dashed lines represent the fitting of the experimental results (symbols) using Eq. (5).

Table 3
Experimental values of K_{O_2} and K_{O_2}' for cells A, B, C, D, E after an overcharge of 1 h at current i

Cell	A	B	C	D	E
i=0.2 A	No data				
K_{O_2} 10^4 (s^{-1})		7.1	4.8	3.7	1.4
K_{O_2}' (cm/h)		0.37	0.25	0.19	0.07
$P_{H_2}^{init}$ (kPa)		62	78	99	77
$P_{O_2}^{init}$ 1(kPa)		7.5	4	13	41
i=0.4 A					
K_{O_2} 10^4 (s^{-1})	4.1	7.1	6.0	3.0	0.9
K_{O_2}' (cm/h)	0.21	0.37	0.31	0.16	0.05
$P_{H_2}^{init}$ (kPa)	143	91	145	138	129
$P_{O_2}^{init}$ (kPa)	38	18	14	54.5	83
i=0.6 A					
K_{O_2} 10^4 (s^{-1})	3.7	6.0	5.5	3.2	0.9
K_{O_2}' (cm/h)	0.19	0.31	0.28	0.17	0.03
$P_{H_2}^{init}$ (kPa)	195	133	148	141	109
$P_{O_2}^{init}$ (kPa)	50	41	24.5	71	124

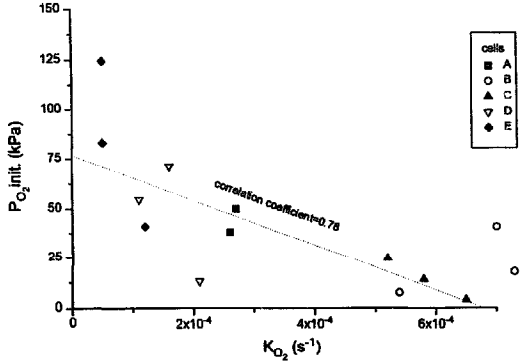

Fig. 6. Correlation between the oxygen reduction rate constant and the initial oxygen pressure after 1 h overcharge.

that for such currents, the recombination mechanism is not significantly modified by the previous overcharge period.

Finally, taking into account the factor-of-merit [6], Γ, which is a convenient parameter related to the geometry of the cell studied, defined as the ratio between the free volume of the experimental setup and the total negative plate surface, roughly estimated to be 0.145 cm (50 cm^3:345 cm^2) in our case, we found that the value of K_{O_2}', defined as $K_{O_2}' = K_{O_2}\Gamma$, is close those reported in Ref. [6], being estimated between 0.02 and 0.1 cm/h.

6.2. Overcharge

Typical curves for hydrogen and oxygen pressure as a function of time are shown in Fig. 7. Hydrogen and oxygen evolution can be obtained by differentiating dP_{O_2}/dt and dP_{H_2}/dt (Figs. 8 and 9).

Three time domains can be observed:

(i) *domain I*: $v_{H_2(rel)} \approx v_{O_2(rel)} \approx 0$ kPa s^{-1}

This may correspond to the recharge of the negative active mass, discharged during the previous rest period. Hydrogen evolution is postponed compared with oxygen evolution. It may be due to the time necessary for oxygen and hydrogen to be formed in the plates and to migrate towards the upper part of the cell before being measured.

(ii) *domain II*: $v_{H_2(rel)}$ and $v_{O_2(rel)}$ increase with time and overcharge current until maximum values $v_{H_2(rel)}^{max}$ and $v_{O_2(rel)}^{max}$ are reached. In most of our experiments, the maximum occurs after 10 to 20 min of overcharge.

(iii) *domain III*: this is the longest domain. Pressure evolution decreases and tends to steady-state values, which are very difficult to determine unambiguously. Longer overcharges should be undertaken in future studies.

Nevertheless, we observed qualitatively that when oxygen reduction is efficient (cells A, B, C, D), the end of charge gas evolutions $v_{O_2(rel)}^{eoc}$ and $v_{H_2(rel)}^{eoc}$ do not depend, as much as

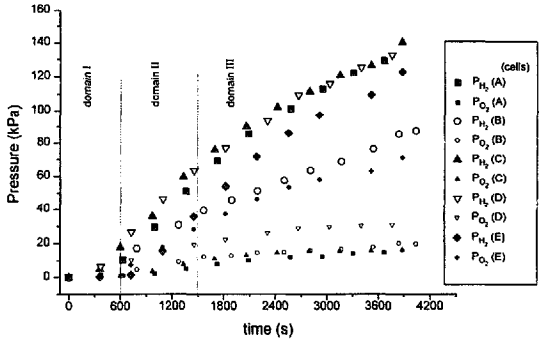

Fig. 7. Hydrogen (large symbols) and oxygen (small symbols) pressures during the 0.4 A overcharge.

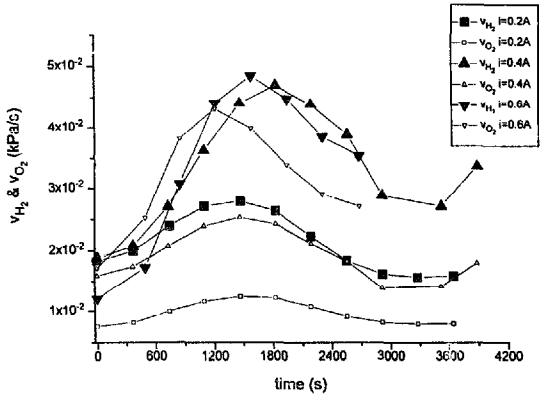

Fig. 8. Hydrogen and oxygen evolution during overcharge, cell E.

does the peak, on the overcharge current and that $v^{\text{exc}}_{O_2(\text{rel})}$ can reach a low value (Fig. 9).

This means that the applied currents, i, are lower than the maximum oxygen reduction ability, i.e. the limiting current $i^{\text{lim}}_{O_2(\text{red})} > i$, and that oxygen reduction efficiency appears to be close to 1.

Thus, cell E exhibits a significantly different behaviour where $v^{\text{exc}}_{O_2(\text{rel})}$ does not tend to low values and depends on i (Fig. 8), since $i^{\text{lim}}_{O_2(\text{red})}$ is lower and $i > i^{\text{lim}}_{O_2(\text{red})}$.

From these figures, it can be seen that, in case B, though the oxygen pressure is similar, the hydrogen pressure is lower than in the other cells, showing the influence of the Forafac 1033D on the hydrogen evolution.

We plot the ratio of $v_{H_2(\text{rel})}/v_{O_2(\text{rel})}$ as a function of time (Fig. 10). As pointed out (Eq. (11)), departure from stoichiometry can easily be assessed. In cell E, the ratio is almost time- and current-constant, and is close to 2. In the other cells, the ratio is higher than 2 and can reach values as high as 10 or 20, though $i_{O_2(\text{rel})}$ is unlikely to be as low as $i_{(\text{misc})}$. As it seems reasonable to assume that the ratio $i_{(\text{misc})}/i_{O_2(\text{rel})}$ (Eq. (9)) is negligible compared to 1, it may have some missing processes or wrong approximations in the equations written in the previous section.

6.3. Correlation between recombination rate and gas emission during overcharge

First, we determined the mean value of hydrogen and oxygen evolution at the end of charge and the corresponding ratio of $v^{\text{exc}}_{H_2(\text{rel})}/v^{\text{exc}}_{O_2(\text{rel})}$ as a function of K_{O_2} (Fig. 11). Fig. 11 shows that the higher is K_{O_2} the higher is the departure from stoichiometry. This is an obvious consequence of Eq. (11) when $v_{O_2(\text{rel})}$ decreases and when the studied system is able to reduce the total amount of oxygen. Unfortunately, though

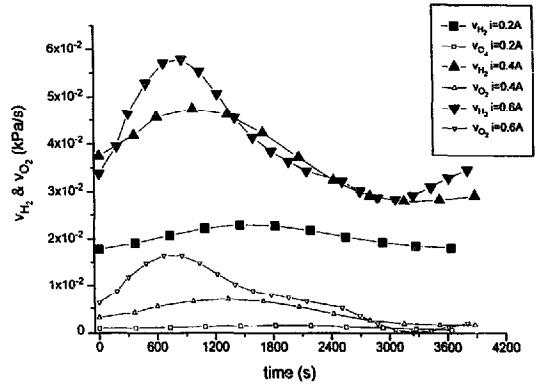

Fig. 9. Hydrogen and oxygen evolution during overcharge, cell C.

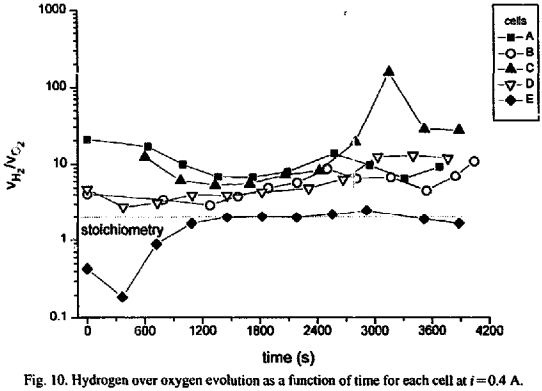

Fig. 10. Hydrogen over oxygen evolution as a function of time for each cell at $i = 0.4$ A.

$v_{O_2(rel)}$ is diminished, $v_{H_2(rel)}$ does not seem to be hindered as much as expected (Fig. 7). Some other unexpected reactions are probably responsible for such behaviour and Eq. (11) is unlikely to be sufficient for explaining this discrepancy.

In addition, Fig. 11 shows that cell B, whose electrolyte contains Forafac 1033D, behaves singularly since it exhibits a good recombinant efficiency and an evolution ratio closer to stoichiometry. This plot confirms that Forafac 1033D appears to be a good hydrogen gassing inhibitor.

6.4. Discussion

As already suggested [6,18], all the oxygen reduced at the negative electrode is not necessarily involved in an electrochemical recombination process. During overcharge or float operations, oxygen recombination can proceed via two possible mechanisms or routes:

(i) Oxygen reacts chemically with lead to form lead sulfate, see reaction (3). The latter can be seen as an oxygen recombination reaction though no external current is related to it, except if following reaction (3), the lead sulfate is reduced

$$PbSO_4 + 2e^- + 2H^+ = Pb + H_2SO_4 \qquad (12)$$

In this case and in this case only, the oxygen cycle is complete, oxygen recombination is achieved and $i_{O_2(rec)} = i_{O_2(red)}$. However, if the lead sulfate is not converted, there is no oxygen recombination and $i_{O_2(rec)} \neq i_{O_2(red)}$.

(ii) Oxygen reacts electrochemically with protons on the lead surface

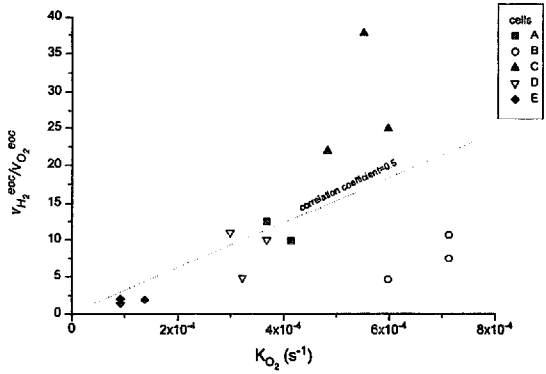

Fig. 11. Correlation between the ratio of hydrogen over oxygen evolution at the end of charge and the oxygen reduction rate constant.

$$\frac{1}{2}O_2 + 2e^- + 2H^+ = H_2O \quad (13)$$

No lead sulfate is formed at the negative plate and the current $i_{O_2(rec)}$ equals $i_{O_2(red)}$.

Relation (9) is valid for either mechanism (i) or (ii). However, it is wrong if the mechanism (i) is not achieved, i.e. the conversion of lead sulfate to lead is not achieved. Consequently, $i_{O_2(red)}$ of Eq. (7) does not equal $i_{O_2(rec)}$ of Eq. (8) and relation (9) is no more valid. Therefore, the quantity of oxygen reduced at the negative electrode is more important than the amount of oxygen recombined such as

$$\Delta i_{O_2} = i_{O_2(red)} - i_{O_2(rec)} \geq 0 \quad (14)$$

then Eq. (9) becomes

$$\frac{i_{H_2(rel)}}{i_{O_2(rel)}} = 1 + \frac{i_{misc}}{i_{O_2(rel)}} + \frac{\Delta i_{O_2}}{i_{O_2(rel)}} \quad (15)$$

It has been claimed [19] that under overcharge current or float operation, the potential of the negative electrodes is too negative for reaction (3) to proceed and that the direct reduction of oxygen (mechanism (ii)) is responsible for recombination mechanism. On the contrary, it has been often experienced [20,21] in VRLA batteries that corrosion of the negative electrode, i.e. sulfation of lugs and plates, can be important during long-term float operation. In recent experiments, we observed on the same type of cells overcharged at low constant current (20 and 100 mA), during one month, that a non-negligible amount of lead sulfate, increasing with the overcharge current, was formed at the top of the negative plates. Obviously, this indicates that the plates — and/or the lug — do not behave in a homogeneous manner and that local drops of potentiel allow reaction (3) to occur.

Oxygen recombination strongly depends on microscopic conditions which may be listed as:

1. Due to the tortuosity of the separator, oxygen bubbles are likely to be driven towards the top of the cell where reaction (3) or (13) takes place preferentially. Likewise, it is possible to assume that the potential at the surface of the plates where oxygen bubbles arrive first can differ from the potential at the mass/negative grid interface. The thicker the plate the higher can be the potential drop between the surface and the core of the plate.
2. Acid stratification [14] can be important in the AGM cell.
3. In a cell made of several negative plates, each plate is not locally submitted to the same oxygen pressure.

All these factors yield important inhomogeneous negative potentials from plate to plate and on the same plate from the bottom to the top and/or from the core to the surface. It is easy to imagine that the isopotential maps of the plates are very complex. We therefore can expect that in some parts of the plate the potential is high enough to allow the sulfation reaction (3) to occur in preference to the conversion reaction (12), leading to a relatively high value of Δi_{O_2} (Eq. (15)).

If route (ii) (reaction (13)) takes place, preferentially at the top of the cell, it will depolarize and increase the sulfation due to self-discharge. Therefore, the question whether mechanism (i) or (ii) is operating during low-current overcharge or float operation remains. Probably, oxygen recombination proceeds via both routes (i) and (ii).

For current balances, hydrogen has to be evolved at sites where the plate has a more negative potential. This mixed potential [16] situation could even lead to electron transfer from the high potential to the low potential parts within the same plate or from plate to plate, resulting in an increase in hydrogen emission and of lead sulfation. Moreover, all these processes are time-dependent since the electrolyte flows and oxygen transport take place in a complex manner. For instance, Musilova and Jindra [17] clearly pointed out the variation of the negative plate potentials during charge.

7. Conclusions

Although this study shows a wide dispersion of data from cell to cell, some interesting conclusions can be drawn.

First, we showed that Raman spectroscopy could be a good experimental method for analysing in situ hydrogen and oxygen evolution in sealed lead/acid batteries. Improving our experimental setup, especially the gas mixing chamber, could be one way to homogenize correctly the gas composition throughout the cell. Up to now, no investigation enabled the continuous determination of gas evolution parameters in lead/acid cells.

Second, we confirmed that the oxygen reduction mechanism followed a first-order kinetic law, at least during the first hour after overcharge and that the values K_{O_2}' were close to those already reported, that is in the order of 0.1 cm/h.

Contrary to the usually admitted behaviour, we showed that hydrogen and oxygen evolution appeared not to be well correlated during short-term low-current overcharges. In all cases, hydrogen evolution was much higher than expected. This observation can be explained by:

(i) *At the positive electrodes, grid corrosion and oxidation of organic species.* Although it is assumed that in standard lead/acid cells, corrosion and oxidation of organic species correspond to insignificant currents, it must be kept in mind when one wants to use new grid alloys and/or new material for the absorptive separator. Further, because the amount of oxygen released tends to very low values after a few hours under float operation, the ratio of $i_{misc}/i_{O_2(rel)}$ can reach values close to unity which henceforth increases the hydrogen compared with oxygen evolution (Eq. (11)).

(ii) *At the negative electrodes, heterogeneous and mixed potentials*, leading to high value of Δi_{O_2}.

In order to prevent too high pressures in sealed AGM lead/acid cells, hydrogen evolution has to be greatly lowered. It may be achieved by oxydation of hydrogen on positive plates using suitable catalysts such as tungsten carbide [22,23] or, according to our discussion, by minimizing the potential heterogeneity throughout the negative plates which is, in our view, probably the main factor responsible for hydrogen gassing and negative plate sulfation. In that way, better care should be addressed on gas transport [2] from positive to negative plate as well as on electrolyte non-uniformity, i.e. specific gravity stratification, plate and/or separator soaking. Another way of reducing hydrogen gassing without modifying oxygen reduction could be to use organic additives such as Forafac 1033D which is very stable in acidic media. Moreover, it results from our observations and assumptions that, under low current overcharge, an efficient oxygen reduction may not be fully favourable for limiting the hydrogen evolution. In this condition, it seems to be a difficult task to make the lead/acid cells sealed.

8. List of symbols

A	parameter as defined in Eq. (10): $A = VF/RT$
A_X	Raman integrated intensity of gas X
C_X	coefficient of proportionnality as defined in Eq. (1)
F	96 500 C
i	total charging current, A
$i_{X(gas)}$	current corresponding to the formation of gas X
$i_{O_2(red)}$	current corresponding to the quantity of oxygen reduced at the negative electrodes
$i_{X(rel)}$	current corresponding to the quantity of gas X released into the empty volume of the element and measured via Raman spectroscopy
$i_{O_2(rec)}$	current corresponding to the oxygen recombination
$i_{O_2(red)}^{lim}$	limiting current for the reduction of oxygen
$i_{(misc)}$	current corresponding to miscellaneous reactions taking place at the positive electrode
K_{O_2}	kinetic rate constant of oxygen reduction as defined in Eq. (4), s^{-1}
K_{O_2}'	defined as $K_{O_2}\Gamma$, cm s^{-1}
$n(t)$	kinetic parameter as defined in Eq. (4)
P_X	partial pressure of gas X, kPa
P_X^{init}	partial pressure of gas X at the end of charge and before the rest period
R	universal gas constant, J K^{-1}
t	time, s
T	absolute temperature, K
$v_{O_2(red)}$	oxygen reduction evolution, kPa s^{-1}
$v_{X(rel)}$	evolution of gas X released into the element free volume and related to $i_{x(rel)}$ via Eq. (10)
$v_{X(rel)}^{max}$	maximum value of $v_{X(rel)}$
$v_{X(rel)}^{moy}$	mean value of $v_{X(rel)}$ at the end of charge
V	volume of the free space available to gas, m^3

Greek letters

Γ	factor-of-merit defined as the ratio of the free space volume of the cell and the surface

Acknowledgements

The authors would like to thank Professor M. Maja (Politecnico di Torino, Italy), Professor J.V. Zanchetta (University of Montpellier, France) and Dr J. Bovet (SAFT, Centre de Recherche Alcatel–Alsthom, Marcoussis, France) for their useful comments and remarks.

References

[1] S.C. Bose and N.A. Hampson, *J. Power Sources, 19* (1987) 261.
[2] J. Mrha, K. Micka, J. Jindra and M. Musilova, *J. Power Sources, 27* (1989) 261.
[3] R.F. Nelson, *J. Power Sources, 31* (1990) 3.
[4] D. Bernt, *Maintenance-Free Batteries, A Handbook of Battery Technology*, Research Studies Press, Taunton, UK, 1993.
[5] W.B. Brecht and D.O. Feder, *Batteries Int.*, (July) (1994) 40.

[6] S. Bodoardo, M. Maja and N. Penazzi, *J. Power Sources, 55* (1995) 183.
[7] B.K. Mahato, E.Y. Weissman and E.C. Laird, *J. Electrochem. Soc., 121* (1974) 13.
[8] J.S. Symanski, B.K. Mahato and K.R. Bullock, *J. Electrochem. Soc., 135* (1988) 548.
[9] H. Dietz, M. Radwan, J. Garche, H. Döring and K. Wiesener, *J. Applied Electrochem., 21* (1991) 221.
[10] CEAC, *Fr. Patent Pend No. 95 05 974* (19 May 1995).
[11] C. Cachet, M. Keddam, V. Mariotte and R. Wiard, *Electrochim. Acta, 39* (1994) 2743.
[12] H. Dietz, G. Hoogestraat, S. Laibach, D. von Borstel and K. Wiesener, *J. Power Sources, 53* (1995) 359.
[13] M. Maja, N. Penazzi and P. Spinelli, *Proc. 6th European Symp. on Corrosion Inhibitors, Ferrara, Italy, 1985*, p. 427.
[14] H. Tuphorn, *J. Power Sources, 46* (1993) 361.
[15] R. Miraglio, L. Albert, A. El Ghachcham, J. Steinmetz and J.P. Hilger, *J. Power Sources, 53* (1995) 53.
[16] J.A. Magyar, M.A. Kepros and R.F. Nelson, *J. Power Sources, 31* (1990) 93.
[17] M. Musilova and J. Jindra, *J. Power Sources, 45* (1993) 325.
[18] S. Hills and D.K.L. Chu, *J. Electrochem. Soc., 116* (1969) 1155.
[19] J.P. Pompon and J. Bouet, 11th Int. Telecommunications Energy Conf., Intelec 89, Florence, Italy, *IEEE Conf. Proc., 2* (1989) 17.4.
[20] S. Atlung and B. Zachen-Christiansen, *J. Power Sources, 52* (1994) 201.
[21] R. Wagner, *J. Power Sources, 53* (1995) 153.
[22] H. Dietz, L. Dittmar, D. Ohms, R. Radwan and K. Wiesener, *J. Power Sources, 40* (1992) 175.
[23] I. Nikolov, G. Papazov and V. Naidenov, *J. Power Sources, 40* (1992) 341.